RSC Advances

ROYAL SOCIETY OF CHEMISTRY

www.rsc.org/advances

Effect of Selective Solvent on the Aggregate Behavior of the Mixed Langmuir Monolayers of PS-*b*-PEO and PS-*b*-PMMA

Zhuang Wang,[1] Gangyao Wen,[1*] Fengyang Zhao,[1] Changchun Huang,[1]

Xiaoqun Wang,[1] Tongfei Shi,[2] and Hongfei Li[2]

[1]*Department of Polymer Materials and Engineering, College of Materials Science and Engineering, Harbin University of Science and Technology, Harbin 150040, P. R. China*
[2]*State Key Laboratory of Polymer Physics and Chemistry, Changchun Institute of Applied Chemistry, Chinese Academy of Sciences, Changchun 130022, P. R. China*

Abstract: A selective solvent was used to study the aggregate behavior of the mixed Langmuir monolayers of polystyrene-*b*-poly(ethylene oxide) (PS-*b*-PEO) and polystyrene-*b*-poly(methyl methacrylate) (PS-*b*-PMMA). A peculiar hysteresis phenomenon is reported for the first time, in which the expansion curves cross their corresponding compression curves, and the final surface pressures after the expansion processes are significantly higher than, instead of close to, their initial compression values. The mixed Langmuir–Blodgett (LB) films exhibit more mixed circular micelles and less mixed rod-like aggregates with the increase of the PS-*b*-PEO content, which is quite different from those only exhibit the mixed circular micelles by using a nonselective solvent. So far we have carried out the progressive morphology evolution and the aggregate density control in the mixed LB films by using the selective spreading solvent and adjusting blend composition and transfer pressure, which is an interesting way to control and design morphology into an ultrathin film for some applications such as nanopatterns and nanotemplates.
Keywords: LB film, block copolymer, polymer blend, selective solvent

Introduction

The aggregation behavior of amphiphilic block polymers at the air/water interface have been widely studied in recent years.[1–18] Most of the previous interface studies focused on the system of polystyrene-*block*-poly(ethylene oxide) (PS-*b*-PEO).[1–9] The formation of PS-*b*-PEO aggregates at the air/water interface has been shown to be a spontaneous process[1,3] and the aggregation morphologies can be affected by many factors such as hydrophilic block length, subphase temperature, and spreading solution concentration.[2–6] Cheyne and Moffitt showed that the spreading concentration could strongly influence the aggregation morphologies and suggested a nonequilibrium mechanism for the formation of various PS-*b*-PEO surface aggregates

---
[*] To whom correspondence should be addressed. Fax: +86 451 8639-2577. E-mail: gywen@hrbust.edu.cn.

starting with an initial dewetting of the copolymer spreading solution from the water surface.[4] Furthermore, some work reported on the interfacial aggregate behavior of polystyrene-*block*-poly(methyl methacrylate) (PS-*b*-PMMA). Seo et al. studied the effects of temperature and molecular weight on the aggregate behavior of PS-*b*-PMMA with very high molecular weight and concluded that the formation of PS-*b*-PMMA surface micelles was compression induced.[10–12]

We once studied the effect of spreading solvents on the Langmuir monolayers and Langmuir–Blodgett (LB) films of polystyrene-*block*-poly(2-vinylpyridine) (PS-*b*-P2VP), and found that the LB films prepared with a nonselective solvent only exhibited isolated circular micelles, while those with a selective solvent exhibited quite different morphologies including planar structure, rod-like structure, circular micelles, and labyrinth pattern, etc.[13] Furthermore, Chung et al. studied the effect of subphase pH on the aggregation behavior of PS-*b*-P2VP at the air/water interface, and found that the formation of a laced network structure at low pH could be understood as a balance of the hydrophobic attraction between the PS cores and the electrostatic repulsion between the ionized P2VP blocks submerged in the water.[14]

Although mixed polymeric LB films are more complex, more and more work has been devoted to their study because it is possible to study the miscibility of polymer blends at the air/water interface and find some new aggregate structures. The mixed polymeric LB films are usually composed of two homopolymers,[19–22] one homopolymer and one diblock copolymer,[23–26] and two diblock copolymers.[27–30] Among the mixed systems of two homopolymers, Kumaki et al. studied the mixed LB films of PMMA and poly(*n*-nonyl acrylate) (PNA), and found that the mixed monolayer was miscible at a low surface pressure but underwent a reversible hierarchical phase separation at a high surface pressure.[19,20]

Among the mixed systems of one homopolymer and one diblock copolymer, we once studied the mixed LB films of homopolystyrene (h-PS) and PS-*b*-P2VP, and obtained the highly uniform and stable necklace-network structures when the h-PS content was 80–95 wt %.[23,24] Lopes et al. studied the mixed LB films of PS and poly(isoprene-*b*-methacrylate) (PI-*b*-PMMA), and found that the effect of PI on PS aggregation gave a new insight into the surface aggregation and could be used to influence the patterning and the dimensions of surface aggregates.[25]

Among the mixed systems of two diblock copolymers, Chang and co-workers prepared the mixed LB films of PS-*b*-P2VP and PS-*b*-PMMA by using the premixed spreading and separate spreading methods.[27] They found that the surface micellization took place rapidly without observable chain exchange among the surface micelles. Seo et al. investigated the mixed LB films of poly(styrene-*b*-ferrocenyl silane) (PS-*b*-PF) and PS-*b*-P2VP by using the above two spreading methods.[28] They found that the structures of the mixed LB films were different from those of the neat copolymers and could be controlled by surface pressure and external electric fields. Moreover, Price et al. studied the mixed LB films of PS-*b*-PEO and polystyrene-*block*-polybutadiene (PS-*b*-PB), and obtained hierarchical structures at the meso- and nanoscales by combining block copolymer microphase separation in the bulk with block copolymer self-assembly at the air/water interface.[29]

In our group, we recently studied the aggregation behavior of the mixed Langmuir monolayers of amphiphilic block copolymers PS-*b*-PEO and PS-*b*-PMMA spread with a nonselective solvent chloroform (good solvent for all the block components), and found that the mixed LB films only exhibited the mixed circular micelles (see Supporting Information, Fig. S1). As mentioned above, furthermore, we really discovered that selective solvent had large effects on the aggregation behavior of the Langmuir monolayers and the morphologies of the LB films of diblock copolymers, e.g., PS-*b*-P2VP, and further pointed out that a block copolymer with a very short hydrophilic block was more likely to be affected by the spreading solvent.[13] In this work, we are mainly interested in the effects of selective solvent toluene (good solvent for PS block but poor solvent for both PEO and PMMA blocks) on the aggregation behavior of the mixed Langmuir monolayers of PS-*b*-PEO/PS-*b*-PMMA and the morphologies of their mixed LB films. Furthermore, the effects of blend composition and transfer pressure on the structures of the mixed LB films are also considered. The Langmuir monolayers and LB films of a symmetric PS-*b*-PEO, an asymmetric PS-*b*-PMMA, and their blends were characterized with the Langmuir film balance technique and atomic force microscopy (AFM), respectively. It is well-known that PS block is surface inactive and water insoluble, PEO block is surface active and water soluble, and PMMA block is surface active but water insoluble. Therefore, the morphologies of the LB films of the symmetric PS-*b*-PEO and the asymmetric PS-*b*-PMMA with short PMMA block prepared with the selective solvent toluene must be quite different, which is beneficial for judging the constitution of the mixed LB films.

Experimental Section

Materials. Two kinds of diblock copolymers used in this study, a symmetric PS-*b*-PEO (SEO19K, M_n(PS) = 9500, M_n(PEO) = 9500, 50 wt % PEO, M_w/M_n = 1.07) and an asymmetric PS-*b*-PMMA (SMMA34K, M_n(PS) = 24 500, M_n(PMMA) = 9000, 26.9 wt % PMMA, M_w/M_n = 1.07), were purchased from Polymer Source Inc. (Canada) and used without further purification. We choose the above codes for the two copolymers, which is convenient for coding the following blends.

Preparation of the Spreading Solutions. Stock solutions of SEO19K and SMMA34K in toluene (HPLC grade, Mallinckrodt), each containing a polymer concentration of 0.50 mg/mL, were prepared. The mixed spreading solutions (0.50 mg/mL) of SEO19K and SMMA34K were prepared by mixing the two stock solutions in different volume ratios, and coded as SEO19K-wt%, i.e., SEO19K-20%, SEO19K-40%, SEO19K-60%, and SEO19K-80% according to the weight fraction of SEO19K. Because the concentrations of the two stock solutions are both 0.50 mg/mL, the weight fraction of SEO19K in a blend is equal to its volume fraction. In order to minimize the experimental error resulted from possible concentration variation, the spreading solutions were given a maximum shelf life of 4 days for isotherm experiments and 7 days for LB film preparation. All the spreading solutions were placed in a refrigerator if not in use, and allowed to equilibrate to room temperature prior to isotherm experiments or LB film preparation.

π–A Experiments. Surface pressure–area (π–A) isotherms of SEO19K,

SMMA34K, and their blends were characterized with a KSV Minitrough (Finland) secured inside a dust shield. The effective area of the trough was 350×75 mm^2. The subphase water (resistivity of 18.2 MΩ·cm) used for the isotherm experiments was purified and deionized with a water purification system (Molecular 1810C, China). In all the isotherm experiments, the subphase temperature was controlled at 25 $^{\circ}$C by using a refrigerated bath circulator (THD-0510, China). The spreading solutions were carefully dropped onto the water surface with a gastight Hamilton mini-syringe. The spreading volumes of SMMA34K, SEO19K-20%, SEO19K-40% and SEO19K-60% were all 20 μL, and those of SEO19K-80% and SEO19K were 15.8 and 13.9 μL, respectively. After complete evaporation of the solvent for 20 min, the Langmuir monolayers were symmetrically compressed with two mobile barriers whose relative speed was 10 mm/min. All the isotherms were run at least two or three times with good reproducibility.

The condition in the hysteresis experiments (compression-expansion cycles) was similar to that in the isotherm experiments. Three maximum pressures, π_{max}, of 5, 10, and 30 mN/m were chosen. When surface pressure reached a maximum value, the barriers were stopped and kept for 30 s. After the expansion was completed, the barriers were kept for 15 min and the procedure was repeated using progressively higher pressures.

Preparation and AFM Characterization of the LB Films. In this study, the Langmuir monolayers of the samples were further transferred onto silicon wafers to obtain the corresponding LB films. The silicon wafers were pretreated to be hydrophilic by mainly using a mixture of deionized water, ammonia–water, and hydroperoxide (5:1:1 in volume), and a mixture of deionized water, hydrochloric acid, and hydroperoxide (6:1:1 in volume) according to the procedure described in our previous paper.[24] The LB films were transferred at different surface pressures of 0.2 or 0.5, and 7 mN/m, and the substrate was withdrawn vertically through the monolayer at a speed of 2 mm/min. Prior to the transfer, the surface pressures were maintained for 20 min. The LB films were allowed to dry in air for at least 24 h at room temperature, and then characterized with a tapping mode AFM (SPA-300, Seiko Instruments Inc., Japan). The scan areas and speeds of the AFM measurements were 2 μm × 2 μm or 4 μm × 4 μm, and 1.0 Hz, respectively.

<center>**Results and Discussion**</center>

π–A **Isotherms**. Fig. 1 shows the π–A isotherms of the Langmuir monolayers of SEO19K, SMMA34K, and their blends. From Fig. 1, it can be seen that the isotherms of the mixed Langmuir monolayers fall between those of neat SMMA34K and neat SEO19K. The isotherms of SMMA34K and SEO19K-20% are featureless and noobvious transition plateaus exist, and surface pressure in the former increases more steeply with a large limiting mean molecular area (A_0 = 24.83 nm^2). The A_0 describing the chain packing density within the densely packed aggregates was determined by extrapolating the steep linear region to the surface pressure of zero.[24] Devereaus and Baker reported that the extent of the pseudoplateau in the PS-b-PEO isotherm was dependent on the PEO content, and found that the PEO pancake-to-brush transition was impeded by the large surface area of the PS cores and no break was observed in
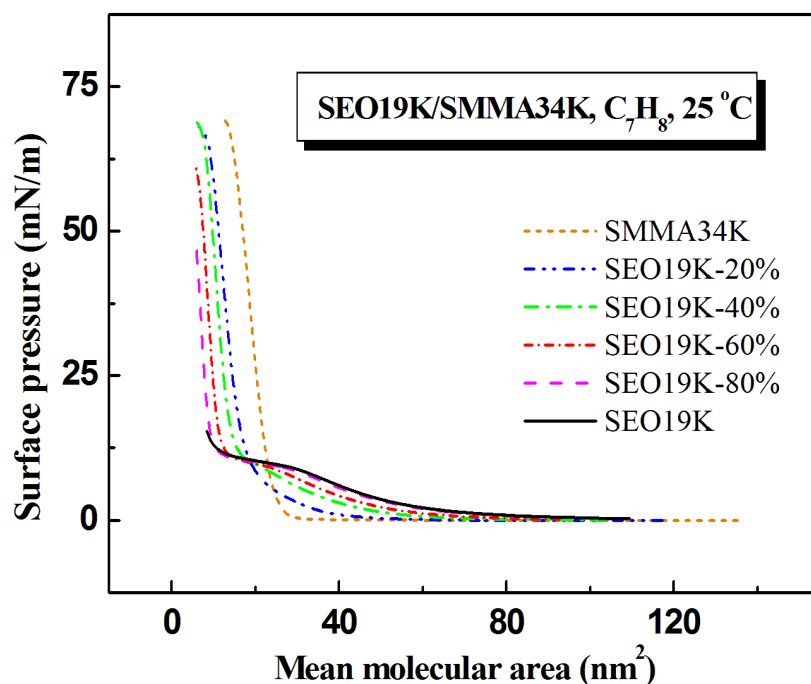
<center>4</center>

Fig. 1 π–A isotherms of the Langmuir monolayers of SEO19K, SMMA34K, and their blends spread with toluene at 25 °C.

the isotherm when the PEO content was less than ~15 wt %.[2] Similarly, the PEO content in our blend SEO19K-20% is 10 wt %, and no obvious transition plateau in the isotherm can be observed. When the SEO19K content is above 40 wt % (20 wt % PEO), however, obvious transition plateaus exist in the isotherms at about 10 mN/m, which is consistent with the pancake-to-brush transition for overlapping PEO blocks upon compression.[4] It is worth noting that surface pressure of the SEO19K monolayer can only reach up to about 15 mN/m until the barriers almost touch the platinum plate during the compression isotherm experiment, which is consistent with that the surface aggregate cores in the monolayer (see Fig. 4c) are too small for surface pressure to further increase.

Table 1 lists some important isotherm parameters obtained from Fig. 1. A_1 and A_2 represent the onset and the end areas of the transition plateaus, respectively.[13] A_{0p} and A_{0b} represent the pancake and the brush limiting areas, respectively.[4] From Table 1, it can be seen that the value of A_1 gradually increases and that of A_2 decreases with the increase of the SEO19K content (above 40 wt %), and thus, the transition plateau region A_1−A_2 becomes wider and wider. It means much more PEO blocks are submerged into water with the increase of the SEO19K content, which is similar to that more surface-adsorbed P2VP blocks occupying much larger molecular areas are submerged into water with the increase of the P2VP block length for the PS-b-P2VP block copolymers reported by us.[13] With the increase of the SEO19K content, therefore, the A_{0p} values of the isotherms increase due to the contribution of PEO blocks, but the A_{0b} values of those decrease mainly due to the contribution of PS blocks. Moreover, the A_{0p} value of SEO19K (~28 Å^2 per EO repeat units) is slightly

lower than that of PS(150 000)-*b*-PEO(35 000) (~31 Å^2) reported by Cheyne,[4] which means the stretching degree of PEO blocks in the former spreads with toluene is a little lower than that in the latter spreads with chloroform. The aggregates retained from the former spreading solution would hinder the stretch of PEO blocks, which is similar to the limited stretching degree of P2VP blocks in the PS-*b*-P2VP monolayer spreads with a selective solvent.[13]

Table 1. Some Important Isotherm Parameters Obtained from Fig. 1[*]

samples	SEO19K-20%	SEO19K-40%	SEO19K-60%	SEO19K-80%	SEO19K
A_1 (nm^2)	—	22.38	24.82	27.79	28.81
A_2 (nm^2)	—	16.40	13.85	12.89	8.48
$A_1 - A_2$ (nm^2)	—	5.98	10.97	14.90	19.33
A_{0p} (nm^2)	33.50	47.98	56.54	63.41	64.35
A_{0b} (nm^2)	18.76	15.60	12.44	11.18	—

*A_1 and A_2 represent the onset and the end areas of the transition region, which are located at the intersections of the extrapolating lines (prior, in, and beyond the transion region). A_{0p} and A_{0b} represent the pancake and the brush limiting areas, which are obtained by the extrapolation of the pancake (3–8 mN/m) and brush regions (12–40 mN/m) in the isotherm to $\pi = 0$, respectively.

Hysteresis Curves. Usually, hysteresis curves are sensitive to the rearrangement or conformation change of polymer chains during the compression-expansion process. In this section, we will present the hysteresis curves of the monolayers of neat block copolymers and their blends, respectively. Fig. 2 shows the hysteresis curves of the Langmuir monolayers of neat SEO19K and neat SMMA34K. There is no hysteresis when the maximum pressure (5 mN/m) is below the transition surface pressure of SEO19K, and the compression and the expansion curves are almost superpose, which is similar to those of other block copolymers.[13,25] When the maximum pressure is 10 mN/m (plateau region), there is a small hysteresis and the final surface pressure is close to the initial compression value. Hysteresis can be quantified by $\Delta A_{0p} = A_{0p} - A'_{0p}$, where A'_{0p} is the pancake limiting area in the expansion isotherm.[4] The ΔA_{0p} value of SEO19K (3.9 nm^2) is larger than that of PS(4000)-*b*-PEO(3950) (2.7 nm^2) reported by Goncalves da Silva,[6] which means the hysteresis of the former spreads with toluene is larger than that in the latter spreads with chloroform. When the maximum pressures are 5 and 10 mN/m, small hystereses both exist in the Langmuir monolayers of SMMA34K. The expansion curves drop sharply at the beginning, and cross their corresponding compression curves at about 0.13 and 0.40 mN/m, respectively, and the final surface pressures reduce to their initial values. That the compression and expansion curves do not superpose is due to the weak hydrophilicity (or hydrophobicity reported in a paper)[10] of PMMA blocks and their possible chain entanglement[25]. For the low and middle maximum pressures, the hysteresis behaviors of SEO19K-20% and SEO19K-80% (not shown here) are similar to those of SMMA34K and SEO19K, respectively.
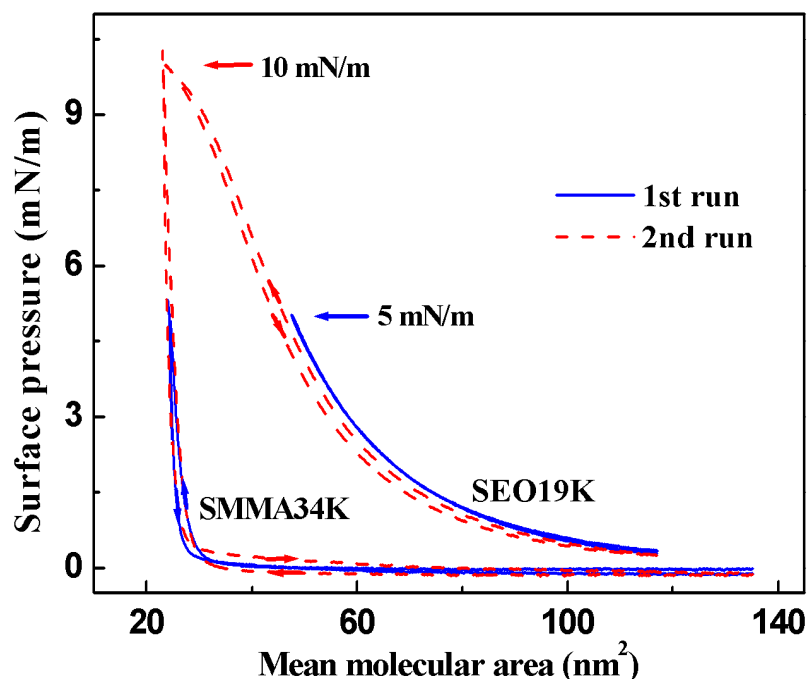
Fig. 2 Hysteresis curves of the Langmuir monolayers of neat SEO19K and neat SMMA34K spread with toluene at 25 °C. The maximum pressures in the 1st and 2nd runs are 5 and 10 mN/m, respectively.

Fig. 3 shows the hysteresis curves of the Langmuir monolayers of SMMA34K, SEO19K-20%, and SEO19K-80%, obtained up to 30 mN/m. No corresponding hysteresis curve of the SEO19K monolayer is given because the corresponding compression isotherm can only reach up to about 15 mN/m. From Fig. 3, it can be seen that obvious hystereses exist for all of these samples. The expansion curves of SMMA34K, SEO19K-20%, and SEO19K-80% cross their corresponding compression curves at 4.5, 9.3, and 11.0 mN/m, and their final surface pressures maintain at about 3.0, 2.4, and 1.6 mN/m, respectively, which are higher than their initial compression values. As far as we know, it is a peculiar hysteresis phenomenon reported for the first time, which can be explained as that some rearrangement occurring with the compression of the monolayer can not fully restore during the expansion process probably due to the weak hydrophilicity of PMMA block and their possible chain entanglements. According to the literatures, however, the final surface pressures in all the hysteresis curves of different block copolymers[6,10,13,16–18,25] and polymer blends[23] were close to their initial compression values. Furthermore, it is worth mentioning that Lopes et al. reported an expansion isotherm of a symmetric PI-*b*-PMMA also crossed the compression curve after compression above the transition regime.[25]
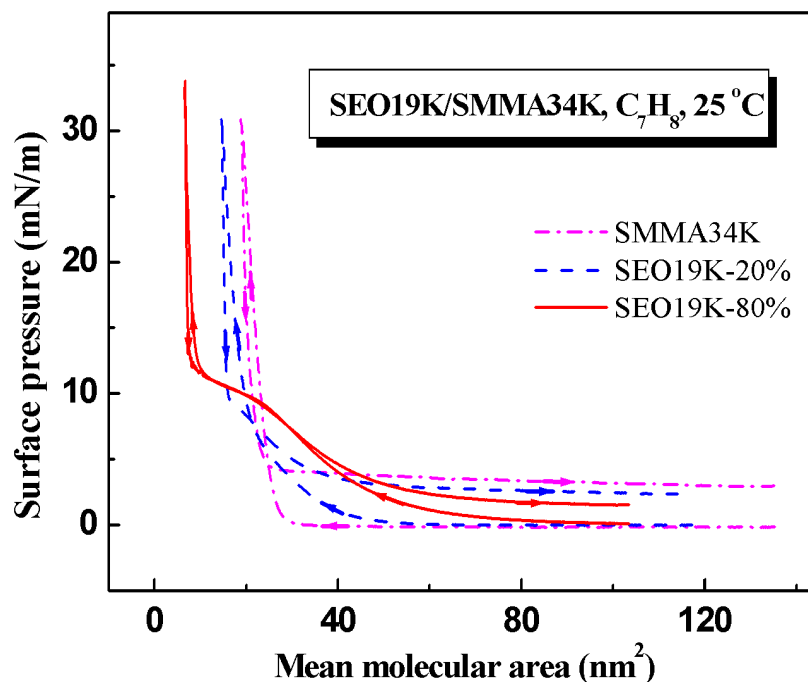
Fig. 3 Hysteresis curves of the Langmuir monolayers of SMMA34K, SEO19K-20%, and SEO19K-80% spread with toluene at 25 ^{o}C. The maximum pressure: 30 mN/m.

The hysteresis in the high surface pressure region can be quantified by $\Delta A_{0b} = A_{0b} - A'_{0b}$, where A'_{0b} is the brush limiting area in the expansion isotherms.[4] The ΔA_{0b} values of SMMA34K, SEO19K-20%, and SEO19K-80% are 4.00, 4.98 and 2.90 nm^2, respectively, which means the hysteresis of SEO19K-80% in the high surface pressure region is smaller than those of SMMA34K and SEO19K-20%. On the other hand, the hysteresis of SEO19K-20% and SEO19K-80% in the low surface pressure region can be quantified by comparing their $|\Delta A_{0p}|$ (the absolute values used here are due to the cross of their expansion and compression curves). The $|\Delta A_{0p}|$ values of SEO19K-20% and SEO19K-80% are 5.23 and 3.37 nm^2, respectively, which means the hysteresis of SEO19K-80% in the low surface pressure region is also smaller than that of SEO19K-20%. For the Langmuir monolayer of SEO19K-80%, shorter sections of more PEO blocks probably immerse into water upon compression due to the high PEO content (40 wt %), and a large amount of the immersed PEO sections can readsorb at the air/water interface during the expansion process due to their strong repulsion in the subphase. While the situation for the SEO19K-20% monolayer is just on the contrary, and thus, the hysteresis of SEO19K-80% is smaller than that of SEO19K-20%. Moreover, the large amount of PMMA blocks in the SEO19K-20% monolayer are compressed more closely and strong PMMA chain entanglements exist in the monolayer, which results in the final surface pressure after the expansion maintains at the higher value than that of SEO19K-80%. It can be seen that PMMA blocks mainly contribute to the surface pressure in the low-pressure region of the expansion isotherms.

AFM Images. Fig. 4 shows the AFM height images of the LB films of neat SMMA34K and neat SEO19K transferred at different pressures. According to the three-dimensional (3D) height images (see Supporting Information, Fig. S2), several luminant domains in panels b–d can be attributed to some dust or silicon oddment introduced during the cutting of the LB films. It is because their heights (as high as 70, 8, and 9 nm in panels b, c, and d, respectively) are obviously larger than those of the predominant aggregates in the corresponding panels (20, 3, and 3 nm, respectively).
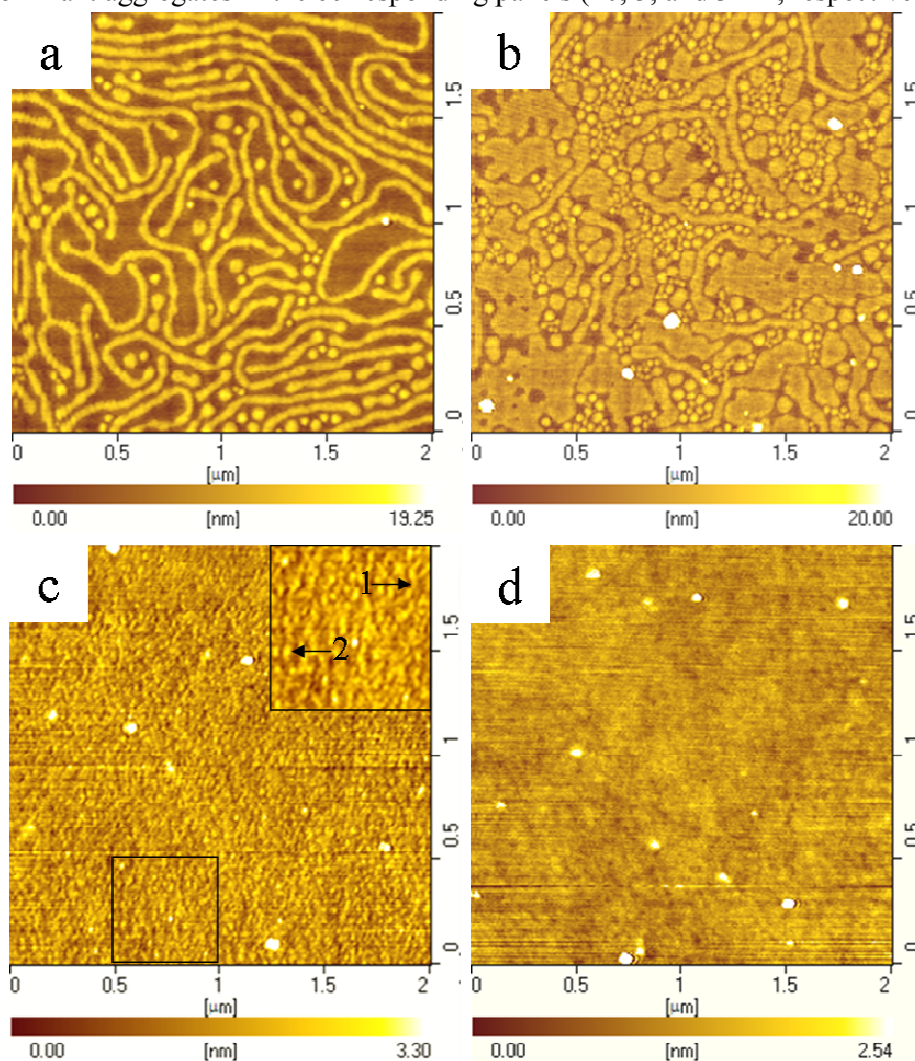

Fig. 4 AFM height images of the LB films of neat SMMA34K (a,b) and neat SEO19K (c,d) transferred at different pressures. The zoom of a small region in black frame is presented in panel c, in which 1 and 2 represent a rod-like aggregate and a circular micelle, respectively. Transfer pressure: 0.2 (a), 0.5 (c), and 7 mN/m (b,d). Scanning area: 2 μm × 2 μm.

Consistent with previous investigations of amphiphilic block copolymers containing hydrophobic PS block at the air/water interface, the raised features in the LB films are attributed to the cores of aggregated PS blocks,[1–4,10–14] which is independent of the spreading solvents. From Fig. 4a, it can be seen that the LB film of SMMA34K transferred at a low pressure exhibits the mixed morphology of predominant rod-like aggregates and few circular micelles.

In our previous paper,[13] solution micelles of PS-*b*-P2VP really existed by using a selective solvent carbon tetrachloride (CCl$_4$) above a critical micelle concentration (as low as 0.02 mg/mL), which was confirmed by dynamic light scattering (DLS). In this paper, the non-polar PS block should be in contact with the non-polar solvent toluene, that is, toluene is selective for PS. Therefore, it is also believed to form the solution micelles of SMMA34K composing of PMMA cores and PS coronas. Han and Mozer studied a PS-*b*-PMMA (M = 291K, 30.3 wt % PS) solution in toluene by small angle neutron scattering and DLS experiments, and suggested that the PMMA block formed the interior core from which the PS block exuded out as an expanded chain.[31] Because of the attraction, PMMA blocks tend to come out from the inner cores of the solution micelles and contact with the water surface to form the coronas of surface micelles when the solution of SMMA34K spreads on the water surface. At the same time, PS blocks tend to leave the water surface and form the cores of the surface micelles because they are incompatible with water and PMMA blocks. However, the aggregates retained from the spreading solution would hinder the stretch of PMMA blocks, which is similar to the limited stretching degree of P2VP blocks in the PS-*b*-P2VP monolayer spreads with a selective solvent.[13] Because the PMMA blocks are short and stretch incompletely on the water surface, many neighboring PS cores tend to fuse into rod-like aggregates which can further fuse into planar structures with the increase of surface pressure (Fig. 4b).

It is also believed to form solution micelles of SEO19K composing of PEO cores[1] and PS coronas due to the interactions among toluene, polar PEO blocks and non-polar PS blocks. According to the above discussion of neat SMMA34K, a quite similar aggregate process will occur for the neat SEO19K monolayer spreads with toluene. The LB film of neat SEO19K transferred at a low pressure (Fig. 4c) exhibits the mixed morphology of circular micelles and rod-like aggregates, whose sizes are very small (about 40 nm in diameter and 3 nm in height) but can still be distinguished according to the inset. The aggregate sizes of SEO19K are much smaller than those of other PS-*b*-PEO,[1–6] which must because the molecular weight of PS block (9500) in SEO19K is very low. Due to the symmetric structure of SEO19K and strong hydrophilicity of PEO, some isolated circular micelles exist in the LB film of SEO19K. At the same time, some rod-like aggregates also exist, which is similar to that of SMMA34K monolayer spreads with toluene. However, Cox et al. studied the LB films of PS$_{140}$-*b*-PEO$_{80}$ and obtained the morphology of totally isolated circular micelles, which was independent of spreading solvent (toluene or chloroform).[1] They admitted that the diblock copolymer solution in chloroform is expected to be predominately in the form of single chains, and micelles with PEO cores are anticipated in toluene. Therefore, they suggested that the polymer must rearrange from its solution configuration when it comes into contact with the water surface. With the increase of transfer pressure, it is strange to see that the LB film of SEO19K exhibits a homogeneous flat film without any obvious aggregates (Fig. 4d). The very small surface aggregates mentioned above (Fig. 4c) disappear and seem to have been embedded in the PEO monolayer upon compression, which we cannot fully understand at the moment.

Fig. 5 shows the AFM height images of the mixed LB films of SEO19K and SMMA34K transferred at different pressures. From Fig. 5, it can be seen that all the mixed LB films mainly exhibit the mixed morphologies of circular micelles and rod-like aggregates. Moreover, some planar structures exist in the LB film of SEO19K-20% transferred at 7 mN/m because the PEO content is too small to prevent some neighboring rod-like aggregates from further fusing into the planar structures. With the increase of the SEO19K content, the mixed LB films exhibit less rod-like aggregates and more circular micelles because more PEO blocks adsorb at the air/water interface and prevent PS cores from further fusing into the rod-like aggregates, and the Z ranges of the mixed LB films decrease due to the short PS block of SEO19K. Moreover, the density of the aggregates tends to increase with the increase of transfer pressure, which can easily be understood that the aggregates come to close upon compression.

According to Figs. 4 and 5, the statistical information of the nanoaggregates transferred at the low surface pressure is listed in Table 2. In the LB film of neat SMMA34K, the diameter and the height of the rods (rod-like aggregates) are about 57 and 13 nm, and those of the circles (circular micelle cores) are about 72 and 16 nm, respectively. In the LB films of neat SEO19K, the diameter and the height of the rods are about 40 and 3 nm, respectively, which are the same as those of the circles. In the mixed LB films of SEO19K and SMMA34K, the diameters of some rods and circles are larger than those of the neat samples, and the heights of the rods and the circles are almost between those of the neat samples, which indicate that the mixed rod-like aggregates and the mixed circular micelles of SEO19K and SMMA34K exist. Furthermore, there are some small circles in the mixed LB films of SEO19K-80%,
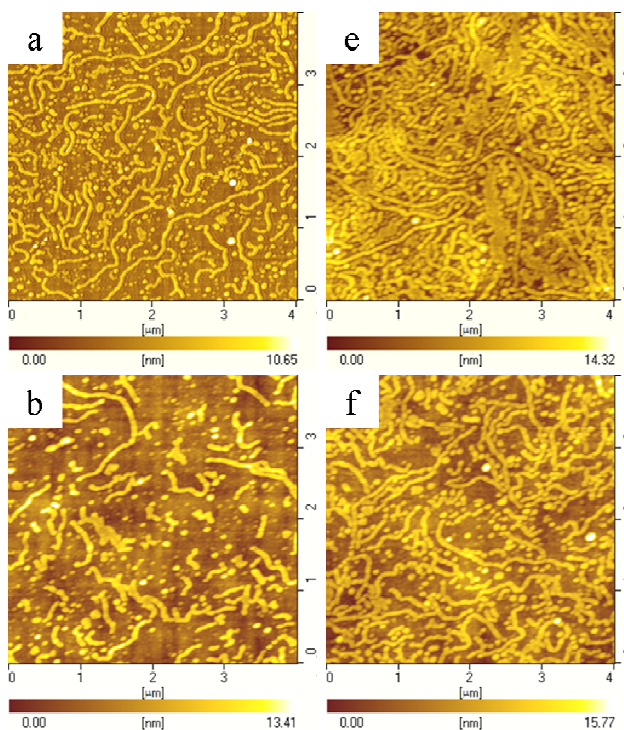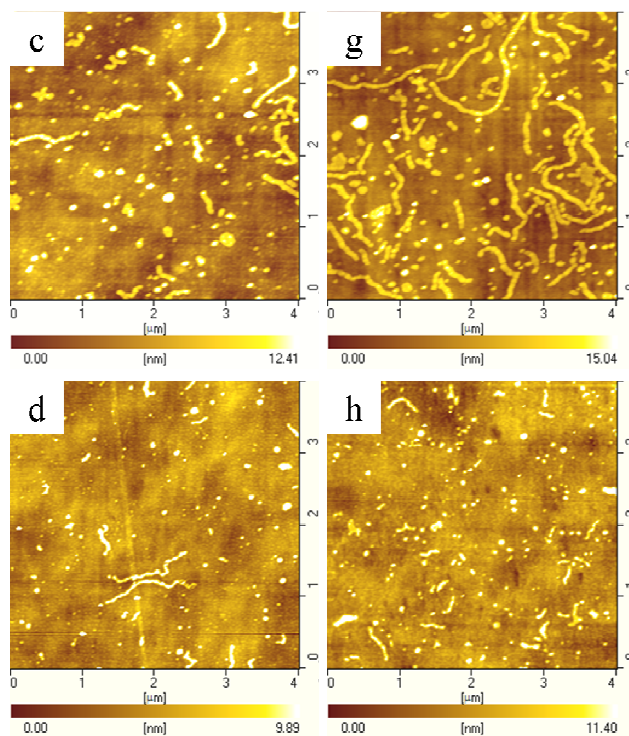
Fig. 5 AFM height images of the mixed LB films of SEO19K and SMMA34K transferred at different pressures. The samples: SEO19K-20% (a,e), SEO19K-40% (b,f), SEO19K-60% (c,g), and SEO19K-80% (d,h). Transfer pressure: 0.2 (a), 0.5 (b-d) and 7 mN/m (e-h). Scan area: 4 μm × 4 μm.

whose diameter and height are 40 and 3 nm, respectively, which represents the existence of circular micelles of neat SEO19K. In the LB films of SEO19K-20%, the diameter and height of some rods are close to those of the LB films of SMMA34K, which represents the existence of some rod-like aggregates of neat SMMA34K.

Table 2. Statistical Information of the Nanoaggregates Transferred at Low Surface Pressures According to Figs. 4 and 5[a]

samples	SMMA34K	SEO19K	SEO19K-20%	SEO19K-40%	SEO19K-60%	SEO19K-80%
D_{rod} (nm)[b]	57 ± 5	40	69 ± 9	100 ± 6	95 ± 8	60 ± 2
h_{rod} (nm)[c]	13 ± 1	3	9 ± 2	11 ± 2	10 ± 1	9 ± 1
D_{circle} (nm)[d]	72 ± 8	40	79 ± 38	65 ± 25	73 ± 21	53 ± 13
h_{circle} (nm)[e]	16 ± 1	3	5 ± 2	8 ± 5	7 ± 4	6 ± 3

[a]Relative standard deviations were obtained from the analysis of many nanoaggregates in the AFM images. [b,c]represent diameter and height of rod-like aggregates, respectively. [d,e]represent diameter and height of circular micelle cores, respectively.

According to the above discussion of neat block copolymers, it is believed to form mixed solution micelles with PS coronas and mixed PEO/PMMA cores (PMMA blocks are found to be miscible with PEO blocks)[32] in the mixed toluene solutions of SEO19K and SMMA34K. Once the mixed solution spreads on the water surface, the hydrophilic PEO and PMMA blocks still tend to come out from the inner cores of the solution micelles and form the coronas of surface micelles, while the hydrophobic PS

blocks tend to leave the water surface and form the cores of the surface micelles. However, the aggregates retained from the spreading solution would hinder the stretch of PEO and PMMA blocks on the water surface due to their entanglement and the rapid evaporation of the solvent. Therefore, the mixed LB films exhibit the structure of mixed rod-like aggregates and mixed circular micelles of SEO19K and SMMA34K with some different sizes. Of course, some neat solution micelles with PEO cores and PS coronas also exist in the mixed solution especially for those with the higher SEO19K content, which results in the existence of the circular micelles of neat SEO19K in the mixed LB films of Fig. 5. More neat solution micelles of SMMA34K with PS coronas and PMMA cores exist in the mixed solutions with the lower SEO19K content, which results in more rod-like aggregates of neat SMMA34K exist in their corresponding LB films.

It is worth mentioning that the mixed LB films of SEO19K and SMMA34K prepared with the nonselective solvent chloroform only exhibit the mixed circular micelles (see Supporting Information, Fig. S1), which is quite different from the results mentioned above. In a chloroform spreading solution, a diblock copolymer exists in the form of random coils because chloroform is a good solvent for both blocks.[25] Cox et al. carried out DLS in PS-*b*-PEO chloroform solutions with various concentrations and found no evidence of micelle formation in the spreading solutions.[1] Seo et al. also demonstrated that no large aggregates existed in a chloroform solution of PS-*b*-PMMA by DLS.[10] Therefore, few micelles exist in the mixed chloroform solution of SEO19K and SMMA34K. When the mixed solution spreads on the water surface, the mixed circular micelles sharing a PS core and mixed corona of PEO/PMMA blocks spontaneously form with the evaporation of chloroform. It is quite similar to the results reported by Chang et al. that PS-*b*-P2VP and PS-*b*-PMMA form mixed micelles sharing a PS core and mixed corona of P2VP and PMMA chains when a premixed chloroform solution spreads at the air/water interface.[27]

Possible Surface Aggregate Evolutions in the Mixed Langmuir Monolayers. According to the above discussion of the hysteresis curves (Fig. 3) and the AFM images (Fig. 5), the possible surface aggregate evolutions in the Langmuir monolayers of SEO19K-20% and SEO19K-80% are taken into account. Fig. 6 schematically illustrates the initial and the final states during the compression process, and the final states after the expansion process of the two samples at the air/water interface. The initial state of the SEO19K-20% Langmuir monolayer (Fig. 6a) is mainly composed of the rod-like aggregates of neat SMMA34K and the isolated mixed micelles of SEO19K and SMMA34K (see Fig. 5a). Upon compression, most of the PEO blocks probably immerse into water due to the low PEO content (10 wt %) in SEO19K-20% and the large amount of PMMA blocks are compressed more closely. It results in the distances between the isolated aggregates in the Langmuir monolayer becoming smaller and smaller (Fig. 6b). The final aggregate distances after the expansion (Fig. 6c) become slightly larger than those in Fig. 6b. It is probably because that only a small amount of the immersed PEO sections readsorb at the air/water interface (due to the weak repulsion between the limited amount of PEO

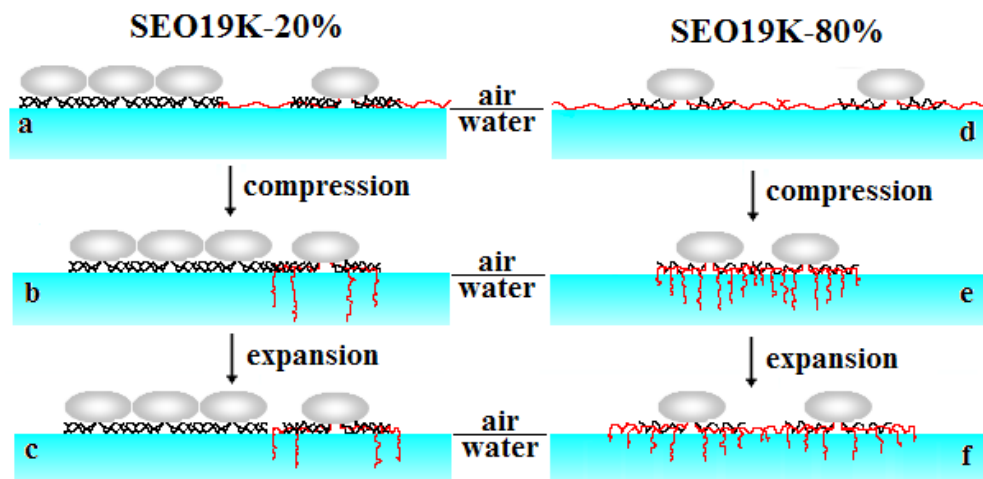blocks in the subphase) and strong PMMA chain entanglements exist in the monolayer.

Fig. 6 Schematic illustrations of the initial (a,d) and the final states (b,e) during the compression process, and the final states (c,f) after the expansion process of SEO19K-20% (a-c) and SEO19K-80% (d-f) at the air/water interface.

On the other hand, the initial state of the SEO19K-80% Langmuir monolayer (Fig. 6d) is mainly composed of the isolated mixed micelles of SEO19K and SMMA34K. Of course, the small amount of neat SMMA34K solution micelles can still transfer to form the sparse and short rod-like aggregates at the air/water interface (according to Fig. 5d). Upon compression, shorter sections of more PEO blocks immerse into water due to the high PEO content (40 wt %) in SEO19K-80% and the small amount of PMMA blocks are not nearly compressed. It results in the aggregate distances slightly decrease (Fig. 6e) and are much larger than those of SEO19K-20% (Fig. 6b). During the expansion process, a large amount of the immersed PEO sections maybe readsorb at the air/water interface due to their strong repulsion in the subphase, which results in the aggregate distances (Fig. 6f) becoming much larger than those of SEO19K-20% (Fig. 6c). The final surface pressure of the SEO19K-20% monolayer is higher than that of SEO19K-80% (see Fig. 3) due to its higher PMMA contents. According to the variation of the aggregate distances, it is possible to explain that the hysteresis of SEO19K-80% is smaller than that of SEO19K-20% (as discussed in Fig. 3).

Conclusions

The Langmuir monolayers and LB films of SEO19K, SMMA34K, and their blends prepared with the selective solvent toluene were studied by using the Langmuir film balance technique and AFM, respectively. The effects of blend composition and transfer pressure on the LB films were also studied. With the increase of the SEO19K content, transition plateaus in the isotherms of the mixed Langmuir monolayers of SEO19K and SMMA34K become wider and wider. A peculiar hysteresis phenomenon is reported for the first time, in which the expansion curves of SMMA34K, SEO19K-20%, and SEO19K-80% cross their corresponding compression curves, and their final surface pressures after the expansion processes are significantly higher than, instead of close to, their initial compression values. The

hysteresis curves show that PEO and PMMA blocks mainly contribute to the surface pressure in the low-pressure region of the compression and expansion isotherms, respectively. Moreover, the lower the SEO19K content is, the larger the hysteresis is.

The LB films of neat SEO19K and neat SMMA34K transferred at low pressures both exhibit the mixed structures of circular micelles and rod-like aggregates, but the latter contains more and longer rod-like aggregates. The mixed LB films exhibit more mixed circular micelles and less mixed rod-like aggregates with the increase of the SEO19K content, which is quite different from those only exhibit the mixed circular micelles by using a nonselective solvent. Moreover, some circular micelles of neat SEO19K also exist in the mixed LB films with the higher SEO19K content and some rod-like aggregates of neat SMMA34K also exist in those with the lower SEO19K content by using the selective solvent. With the increase of transfer pressure, the density of the aggregates in all the mixed LB films tends to increase, and some planar structures exist in the LB films of SMMA34K and SEO19K-20%. Finally, a reasonable schematic illustration is presented to describe the surface aggregate evolutions of the mixed Langmuir monolayers, which can be used to explain the conclusions obtained from the hysteresis curves. So far we have carried out the progressive morphology evolution and the aggregate density control in the mixed LB films by using the selective spreading solvent and adjusting blend composition and transfer pressure, which is an interesting way to control and design morphology into an ultrathin film for some applications such as nanopatterns and nanotemplates.

Acknowledgements

Supporting Information Available: AFM height images of the mixed LB films of SEO19K and SMMA34K prepared with a nonselective solvent chloroform. 2-D AFM height and phase images, and 3-D height image of the LB film of SMMA34K. These materials are available free of charge via the journal homepage.

References

(1) J. K. Cox, K. Yu, B. Constantine, A. Eisenberg and R. B. Lennox, *Langmuir*, 1999, **15**, 7714−7718.

(2) C. A. Devereaux and S. M. Baker, *Macromolecules*, 2002, **35**, 1921−1927.

(3) R. B. Cheyne and M. G. Moffitt, *Langmuir*, 2005, **21**, 5453−5460.

(4) R. B. Cheyne and M. G. Moffitt, *Langmuir*, 2006, **22**, 8387−8396.

(5) C. P. Glagola, L. M. Miceli, M. A. Milchak, E. H. Halle and J. L. Logan, *Langmuir*, 2012, **28**, 5048−5058.

(6) A. M. Goncalves da Silva, A. L. Simoes Gamboa, and J. M. G. Martinho, *Langmuir* 1998, 14, 5327−5330.

(7) S. Harirchian-Saei, M. C. P. Wang, B. D. Gates and M. G. Moffitt. *Langmuir*, 2010, **26**, 5998−6008.

(8) L. Deschenes, M. Bousmina and A. M. Ritcey. *Langmuir*, 2008, **24**, 3699−3708.

(9) S. M. Baker, K. A. Leach, C. E. Devereaux and D. E. Gragson. Macromolecules, 2000, **33**, 5432−5436.

(10) Y. Seo, J. H. Im, J. S. Lee and J. H. Kim, *Macromolecules*, 2001, **34**, 4842–4851.

(11) Y. Seo, K. Paeng and S. Park, *Macromolecules*, 2001, **34**, 8735–8744.

(12) Y. Seo, C. Y. Cho, M. Hwangbo, H. J. Choi and S. M. Hong, *Langmuir*, 2008, **24**, 2381–2386.

(13) G. Wen, B. Chung and T. Chang, *Polymer*, 2006, **47**, 8575–8582.

(14) B. Chung, M. Choi, M. Ree, J. C. Jung, W. C. Zin and T. Chang, *Macromolecules*, 2006, **39**, 684–689.

(15) E. Glynos, S. Pispas and V. Koutsos, *Macromolecules*, 2008, **41**, 4313-4320.

(16) X. Wang, X. Ma and D. Zang, *Soft Matter*, 2013, **9**, 443–453.

(17) H.-W. Park, J. Choi, K. Ohn, H. Lee, J. W. Kim, Y.-Y. Won. *Langmuir*, 2012, **28**, 11555–11566.

(18) T. J. Joncheray, K. M. Denoncourt, M. A. R. Meier, U. S. Schubert and R. S. Duran. *Langmuir*, 2007, **23**, 2423–2429.

(19) Y. Sasaki, N. Aiba, H. Hashimoto and J. Kumaki, *Macromolecules*, 2010, **43**, 9077–9086.

(20) K. Sugihara and J. Kumaki, *J. Phys. Chem. B*, 2012, **116**, 6561–6568.

(21) J. Liu, Y. Zhang, J. Zhang, D. Shen, Q. Guo, I. Takahashi and S. Yan, *J. Phys. Chem. C*, 2007, **111**, 6488–6494.

(22) C. Bernardini, M. A. Cohen Stuart, S. D. Stoyanov, L. N. Arnaudov and F. A. M. Leermakers, *Langmuir* 2012, **28**, 5614–5621.

(23) G. Wen, B. Chung and T. Chang, *Macromol. Rapid Commun.*, 2008, **29**, 1248–1253.

(24) G. Wen, *J. Phys. Chem. B*, 2010, **114**, 3827–3832.

(25) S. I. C. Lopes, A. M. P. S. Goncalves da Silva, P. Brogueira, S. Picarra and J. M. G. Martinho, *Langmuir*, 2007**, 23**, 9310–9319.

(26) S. Yang, X. Yu, L. Wang, Y. Tu, J. X. Zheng, J. Xu, R. M. V. Horn and S. Z. D. Cheng, *Macromolecules*, 2010, **43**, 3018–3026.

(27) B. Chung, H. Choi, H. W. Park, M. Ree, J. C. Jung, W. C. Zin and T. Chang, *Macromolecules*, 2008, **41**, 1760–1765.

(28) Y.-S. Seo, K. Kim, A. Galambos, R. Lammertink, G. Vancso, J. Sokolov and M. Rafailovich, *Nano Lett.*, 2004, **4**, 483–486.

(29) E. W. Price, Y. Guo, C. W. Wang and M. G. Moffitt, *Langmuir*, 2009, **25**, 6398–6406.

(30) D. Xie, C. A. Rezende, G. Liu, S. Pispas, G. Zhang and L. T. Lee, *J. Phys. Chem. B*, 2009, **113**, 739–744.

(31) C. C. Han and B. Mozer, *Macromolecules*, 1977, **10**, 44–51.

(32) W.-P. Hsu, *Colloids and Surface A: Physicochem. Eng. Aspects*, 2010, **367**, 161–166.

Table of Contents
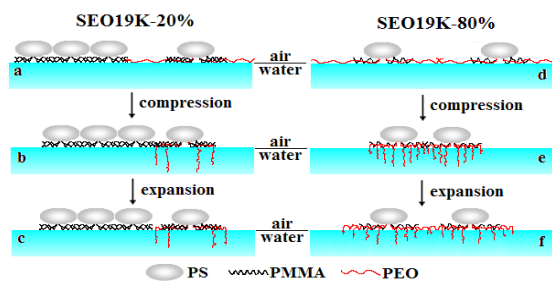
A peculiar hysteresis phenomenon is reported in the mixed Langmuir monolayer of PS-*b*-PEO and PS-*b*-PMMA